

# Supporting Information

## Scalable Exfoliation Process for Highly Soluble Boron Nitride Nanoplatelets by Hydroxide-Assisted Ball Milling

*Dongju Lee,<sup>†</sup> Bin Lee,<sup>†</sup> Kwang Hyun Park,<sup>†</sup> Ho Jin Ryu,<sup>‡</sup> Seokwoo Jeon,<sup>\*†</sup> and Soon Hyung  
Hong<sup>\*†</sup>*

<sup>†</sup>Department of Materials Science and Engineering, Graphene Research Center (GRC), and  
KAIST Institute for the NanoCentury, Korea Advanced Institute of Science and Technology  
(KAIST), Daejeon, 305-701, Republic of Korea

<sup>‡</sup>Department of Nuclear and Quantum Engineering, Korea Advanced Institute of Science and  
Technology (KAIST), Daejeon, 305-701, Republic of Korea

\*Corresponding author

Prof. Seokwoo Jeon: [jeon39@kaist.ac.kr](mailto:jeon39@kaist.ac.kr)

Prof. Soon H. Hong: [shhong@kaist.ac.kr](mailto:shhong@kaist.ac.kr)

## Experimental

### S1. Materials

h-BN powder and sodium hydroxide were purchased from Kojundo Korea Co., Ltd and Junsei Chemical Co., Ltd., respectively. Hydrochloric acid (HCl), methanol (MeOH), Ethanol (EtOH), dimethylformamide (DMF), N-Methyl-2-pyrrolidone (NMP), chloroform, xylene, oleylamine and linear low-density polyethylene (LLDPE) were purchased from Sigma-Aldrich. Isopropyl alcohol (IPA) was purchased from Merck.

### S2. Methods

#### *Exfoliation of hexagonal boron nitride by hydroxide-assisted ball milling (OH-BNNPs)*

A horizontal planetary mill (Fritsch Pulverisette 5) was used for exfoliation. Then, 2 g of micron-sized h-BN powder (used as received, see Figure S1) and a 2 M aqueous NaOH solution were loaded into a steel grinding bowl with 8-mm-diameter steel balls at ball-to-powder ratio of 50:1. The rotational speed of the planetary mill was set to 200 rpm, and the h-BN/NaOH solution mixture was milled for 24 hours. The milled product was collected and rinsed with HCl solution (100 ml) to remove the remaining residual like  $\text{Fe}^{3+}$  and repeatedly washed with and deionized (DI) water until the pH was close to neutral. The samples were dried in a vacuum oven and dispersed in IPA at an initial concentration of 0.5 mg/ml and sonicated for 1 hour. The dispersed BN solution was centrifuged at 2000 rpm for 30 minutes to remove the aggregated material and thick flakes.

#### *Functionalization of OH-BNNPs and preparation of nanocomposites*

Nanocomposites were prepared via a simple and efficient noncovalent functionalization route and solution mixing process. The exfoliated OH-BNNPs (1 mg/ml) were mildly sonicated for 2 hours in xylene solution containing 0.25 (v/v) oleylamine (70%). The oleylamine-functionalized OH-BNNPs (*f*-BNNPs) was washed with ethanol. The as-prepared

f-BNNPs were again dispersed in 75 ml of xylene. Then, 3 g of linear low-density polyethylene (LLDPE) was added to the dispersion and dissolved using stirring at 140°C to obtain a viscous solution. A coagulated polymer nanocomposite was obtained by adding the solution dropwise into a large volume of vigorously stirred methanol. The coagulated nanocomposite powder was isolated via filtration, washed with methanol, and dried at 70°C in a vacuum oven for 10 hours to remove the residual solvent, antisolvent, and moisture. The polymer nanocomposite powders were then compression molded at 15 MPa and 140°C. The aluminized polyethylene film for control experiment was prepared by sputtering Al onto a polyethylene film. The thickness of deposited Al was approximately 700 nm.

### S3. Equipment and techniques

The morphology of OH-BNNPs was investigated using atomic force microscopy (AFM) (Seiko Instrument, Inc.) in tapping mode under ambient conditions. Transmission electron microscopy (TEM) (JEOL JEM-2200FS) analyses were also carried out. Samples for AFM and TEM were prepared by drying a droplet of the OH-BNNPs suspension on a mica substrate and Lacey carbon grid. Field-emission scanning electron microscopy (SEM) (Hitachi S4800) was used to study the morphology of the nanocomposites. The crystallographic structures of the samples were analyzed by X-ray diffraction (D/MAX-2500 (18kW)) with Cu K $\alpha$  radiation ( $\lambda=1.518$  Å). UV–vis spectra were measured to evaluate the dispersion concentration using a UV-3101PC spectrometer. The surface functional groups of the samples were measured by Fourier transform infrared (FT-IR) spectra (Jasco FT/IR-4100 type-A spectrometer, ATR mode) and X-ray photoelectron spectroscopy (Sigma Probe, Thermo VG Scientific, AlK $\alpha$ ). The oxygen and water vapor permeability of the nanocomposites (with a sample size of  $5 \times 5$  cm<sup>2</sup>) was characterized via transmission rate analysis according to ASTM D3895 (MOCON, OX-TRAN Model 2/21) and ASTM F1249 (MOCON, PERMATRAN-W MODEL 3/33), respectively. The nanocomposite films, which

were  $0.70 \pm 0.02$  mm thick, were masked using adhesive aluminum foil to define a surface area of  $5 \text{ cm}^2$ . The oxygen permeability was measured at  $23^\circ\text{C}$ , and the water vapor permeability was measured at  $38^\circ\text{C}$ , both with a relative humidity of  $90 \pm 5\%$ . The response to tensile loading was measured using a universal testing machine (INSTRON 8848 Microtester) according to ASTM D882-10, with a crosshead speed of  $30 \text{ mm/min}$  at room temperature.

### Characterization

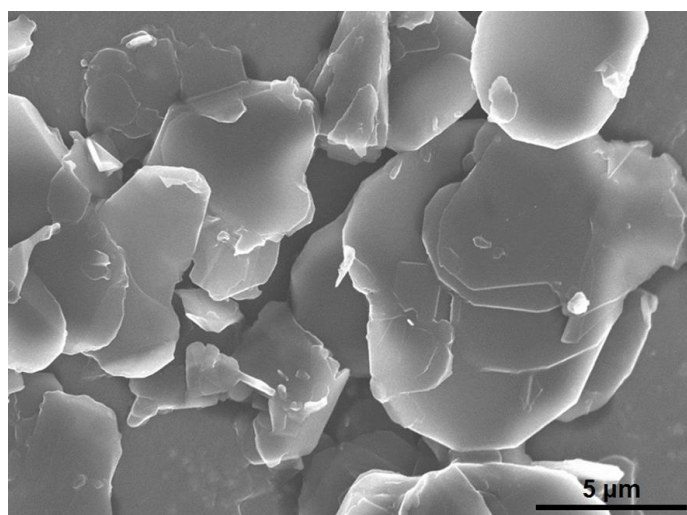


**Figure S1.** As-received h-BN powders.

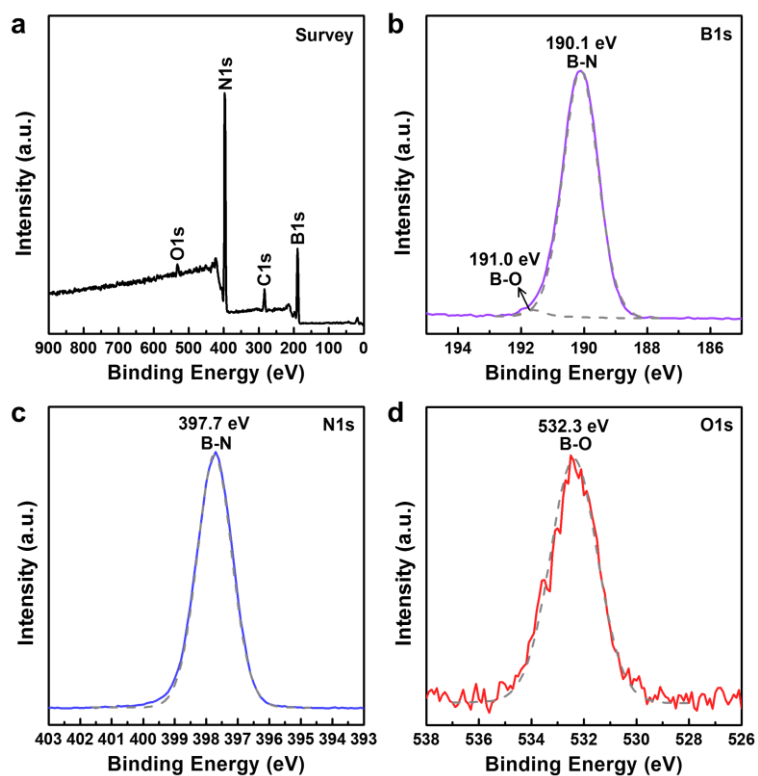


**Figure S2.** a) XPS survey scan of as-received h-BN powders on a Si substrate. b) B1s XPS spectra, c) N1s XPS spectra, d) O1s XPS spectra.

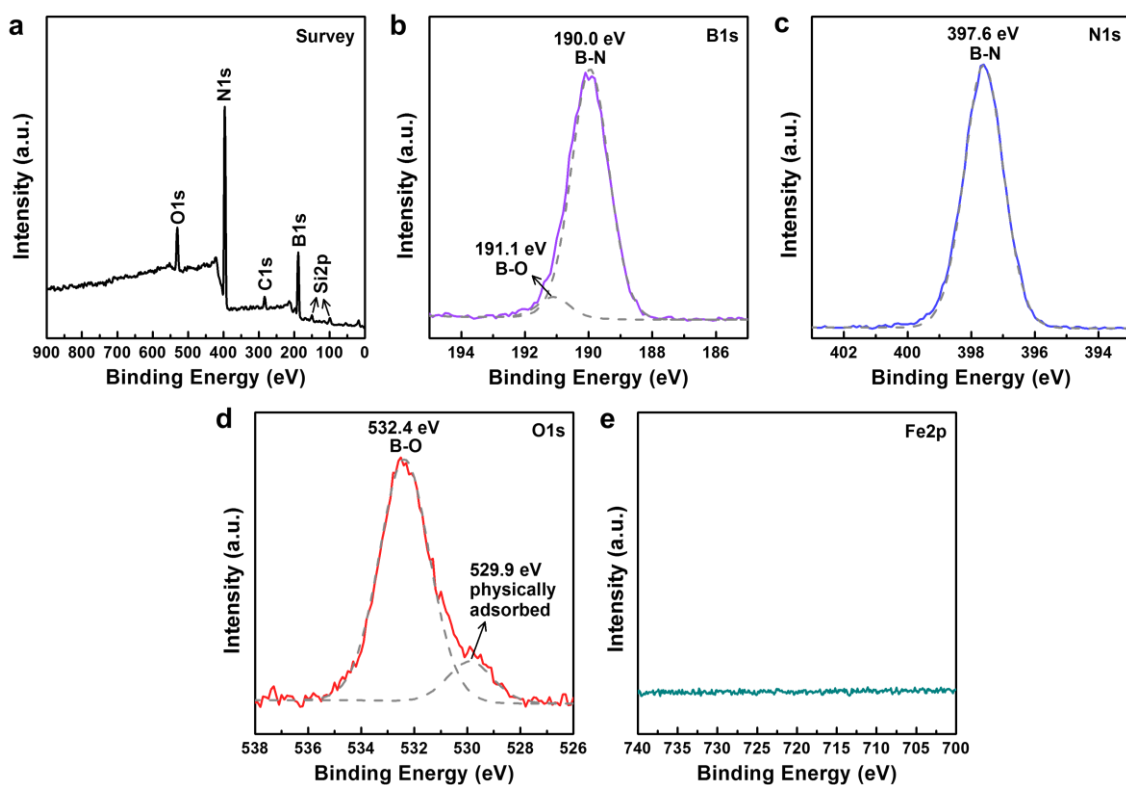


**Figure S3.** a) XPS survey scan of the OH-BNNP samples on a Si substrate. b) B1s XPS spectra, c) N1s XPS spectra, d) O1s XPS spectra, e) Fe2p XPS spectra.

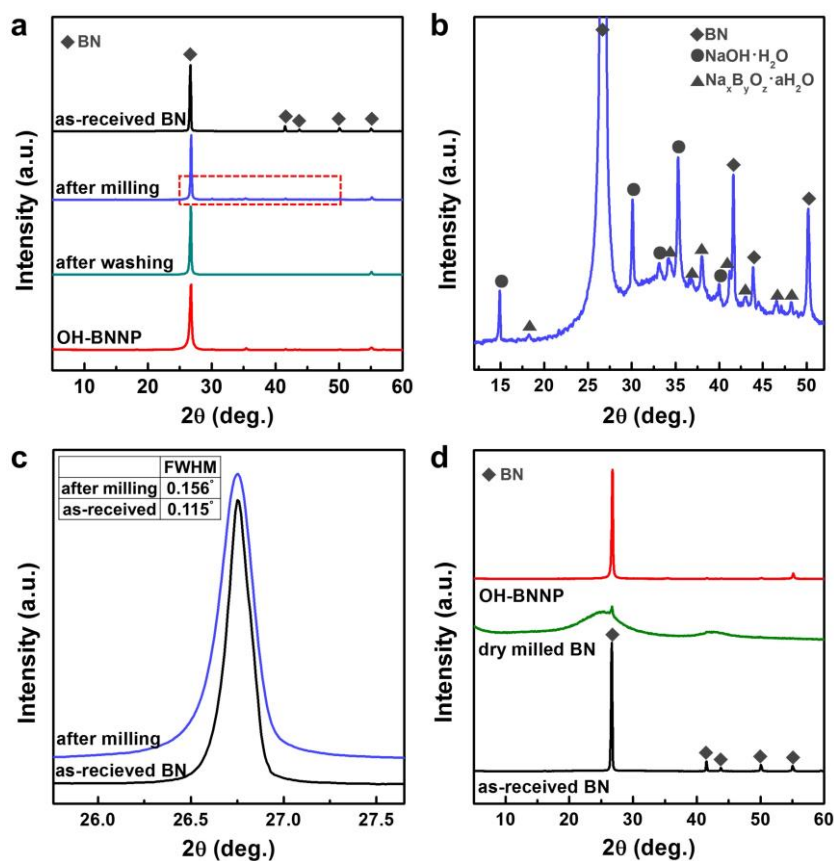
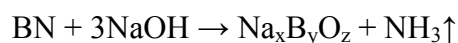


**Figure S4.** a) XRD spectra of the samples following each of the process steps. b) Enlarged XRD spectra of the BN powders after milling. c) XRD spectra and the full-width at half-maximum (FWHM) of the (002) plane peak following milling. d) XRD spectra of the as-received BN, dry-milled BN, and OH-BNNPs. Severe degradation of the crystallinity of BN occurred following dry milling.

The XRD results show that complex sodium boroxide phases were present following milling, as shown in Figure S4a and S4b. Additionally, a strong odor of ammonia was noted when the steel grinding bowl was opened. The formation of these sodium boroxide phases and ammonia gas is attributed to the following reaction of h-BN and sodium hydroxide:



In the XRD spectra, the (002) plane peak of BN (26.7°) was preserved following each process step, and the full-width at half-maximum (FWHM) of the (002) plane peak changed only marginally following milling (from 0.115° to 0.156°). There was little damage to the in-plane

structure following the milling process (see Figure S4c). Consequently, the cutting of h-BN sheets is attributed to the reaction of h-BN and the hydroxide ions at the boron–nitrogen bonds near defect sites, which then propagates when adjacent borazine units are hydroxylated, eventually reaching the edges of the parent particle. The loss of crystallinity in the BN was much less significant than it was with dry milling because of the reduced impact energy due to the liquid controlling agent (see Figure S4d).

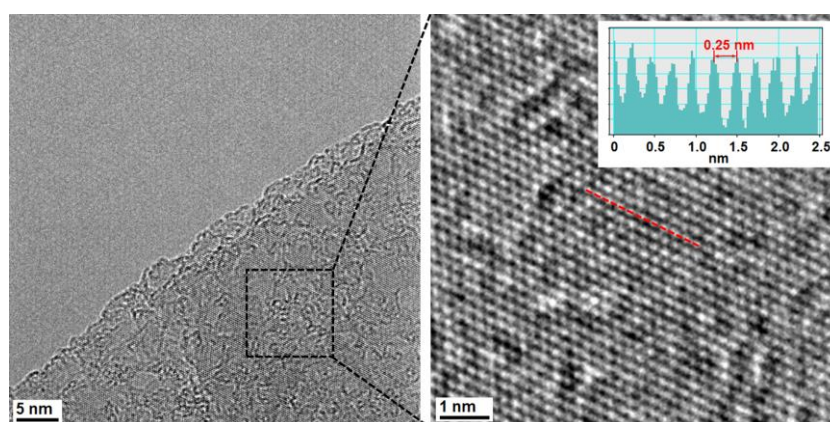


**Figure S5.** High-resolution TEM images of the OH-BNNP. TEM contrast intensity profile recorded along the marked red line, indicating that the fringe separation was  $\sim 0.25$  nm.

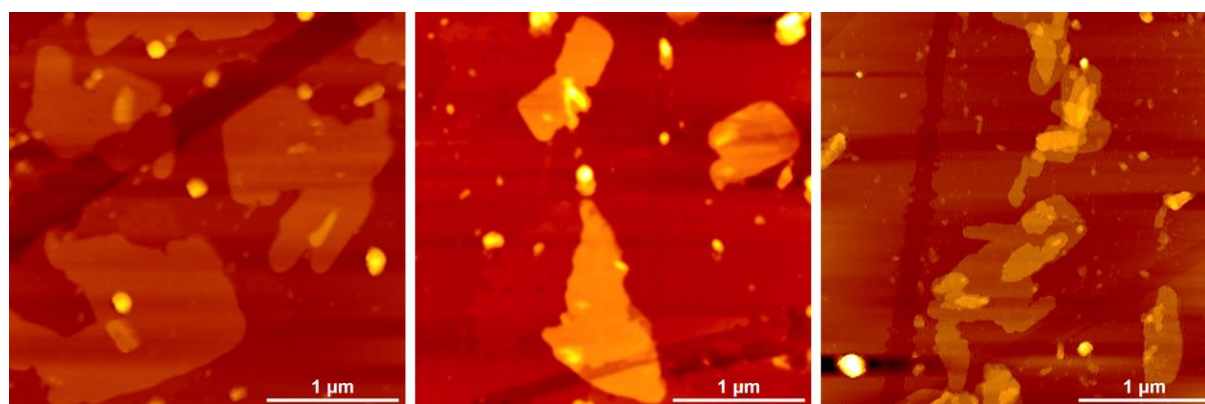


**Figure S6.** AFM topography image of OH-BNNPs with wrinkle-free and smooth over large areas.

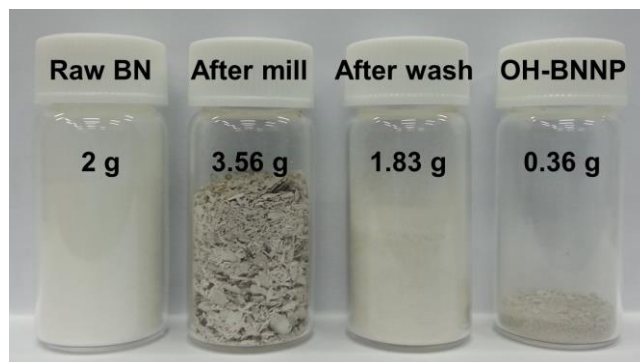


**Figure S7.** Photographs of the samples following each process step.

### **Sediment recycling test**

As shown in the main paper, the yield of exfoliated BNNPs is 18%. In order to demonstrate BN sediment that is removed by centrifugation can be reused, we mixed the sediment with fresh NaOH solution and ball milling once again in the same experimental conditions. After washing and centrifuging the dispersions in IPA for 30 min at 2000 rpm, the recycled BNNP samples were analyzed by TEM, AFM and XPS. A 0.14 g of BNNPs was exfoliated giving a yield of 7% after second milling. TEM and AFM results reveal that BNNPs produced from the sediment have relatively smaller lateral size than that produced from fresh BN powders as shown in Figure S8. XPS spectra of recycled BNNP samples are shown in Figure S9. The degree of hydroxylation after recycling test is comparable to first cycle.

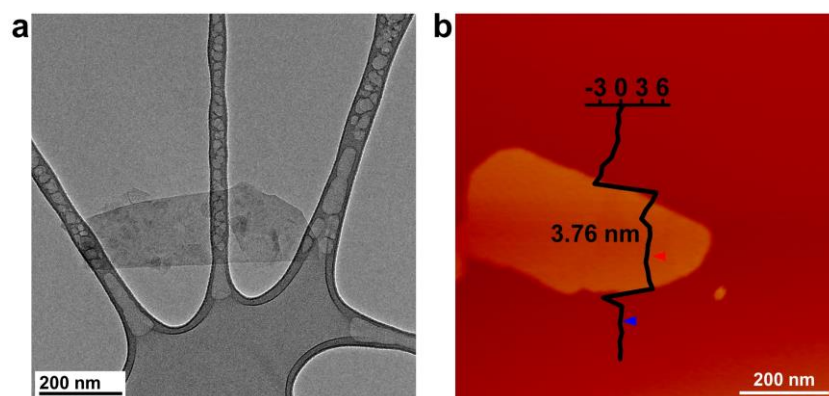


**Figure S8.** a) Low-magnification TEM image and b) AFM topography image of recycled BNNP samples.

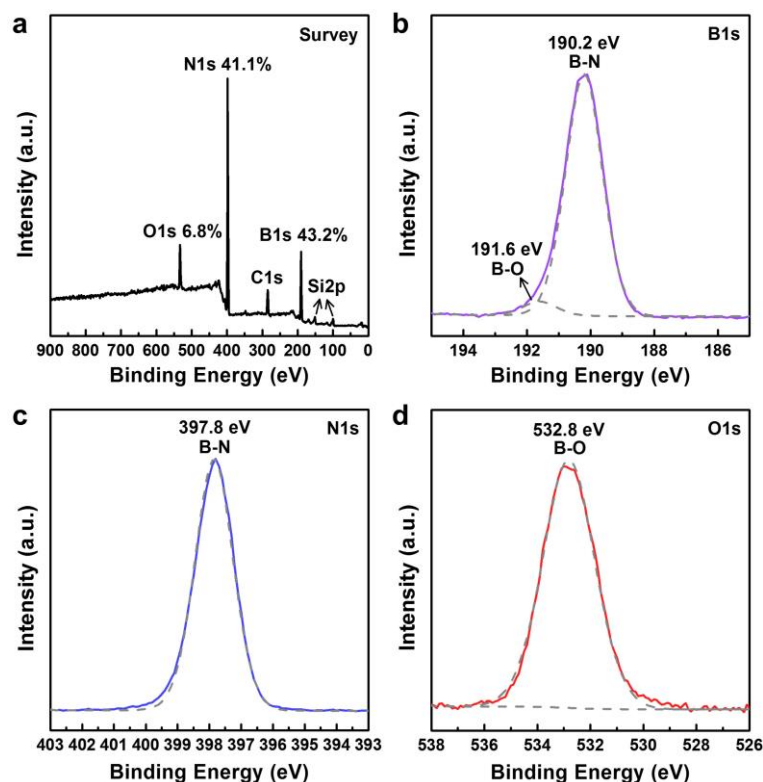


**Figure S9.** a) XPS survey scan of recycled BNNP samples. b) B1s XPS spectra, c) N1s XPS spectra, d) O1s XPS spectra.

### Dispersion stability and optical characterization

OH-BNNPs were dispersed in water and 7 organic solvents to a nominal concentration of 1 mg/ml with the aid of bath ultrasonication, and the dispersions were then allowed to settle for 1 week. Figure S10a shows digital photograph of all dispersions immediately after sonication (top) and 1 weeks after sonication (bottom). For OH-BNNPs dispersions in three organic solvents (IPA, DMF and NMP) were seen to exhibit long-term stability.

To calculate remaining concentration, the dispersions were filtered through Anodisc inorganic membranes (0.1  $\mu\text{m}$  nominal pore size) of known mass. The membranes were dried and the mass of deposited material measured. This allowed the calculation of the actual mass that had been dispersed in the dispersion. Given that the filtered volume was known, we could calculate that the concentration. The as-prepared dispersions were then serially diluted to create a dilution series. The absorption spectra for diluted dispersions are measured.

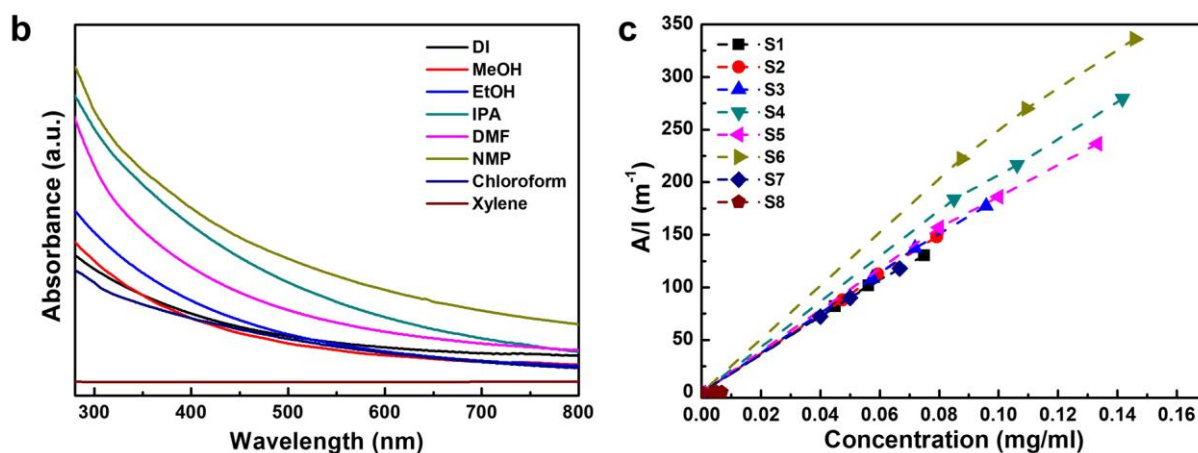
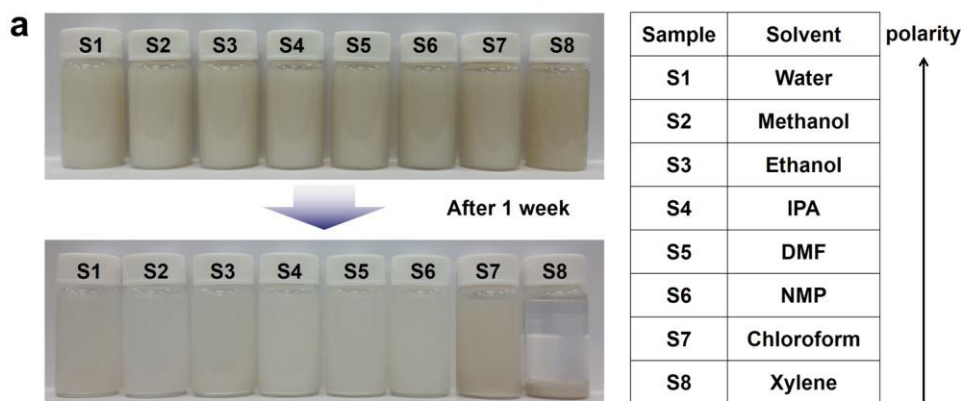


**Figure S10.** a) Digital photograph images of OH-BNNPs suspensions in diverse solvents for 1 week after sonication. b) Optical absorption spectra for dispersions. c) Optical absorbance slopes at excitation wavelength 300 nm as a function of the OH-BNNPs concentration in the each solvent showing Lambert-Beer behavior.

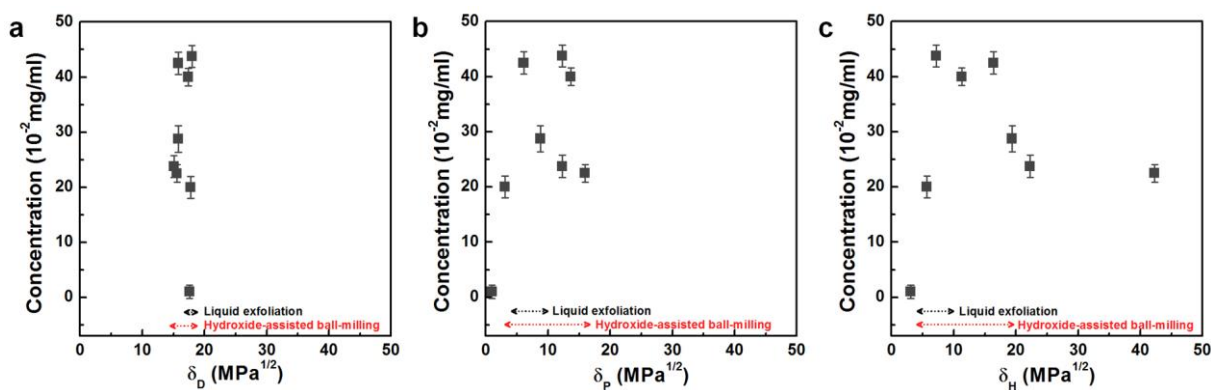


**Figure S11.** Dispersed concentration of OH-BNNPs plotted as a function of the a) dispersive, b) polar, and c) H-bonding Hansen parameters.

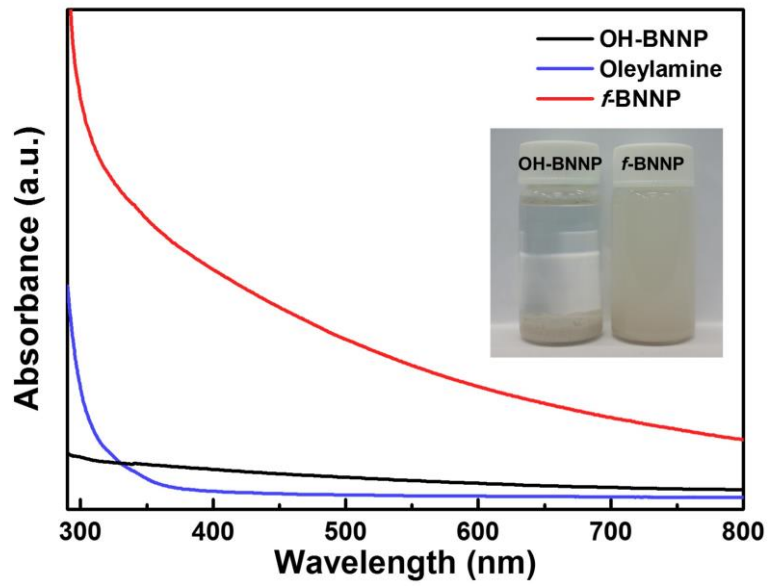


**Figure S12.** UV-vis spectra of suspensions of OH-BNNPs and oleylamine functionalized OH-BNNPs (*f*-BNNPs) in xylene, all following settling for 1 day. The inset shows photographs of suspensions of OH-BNNPs and *f*-BNNPs.

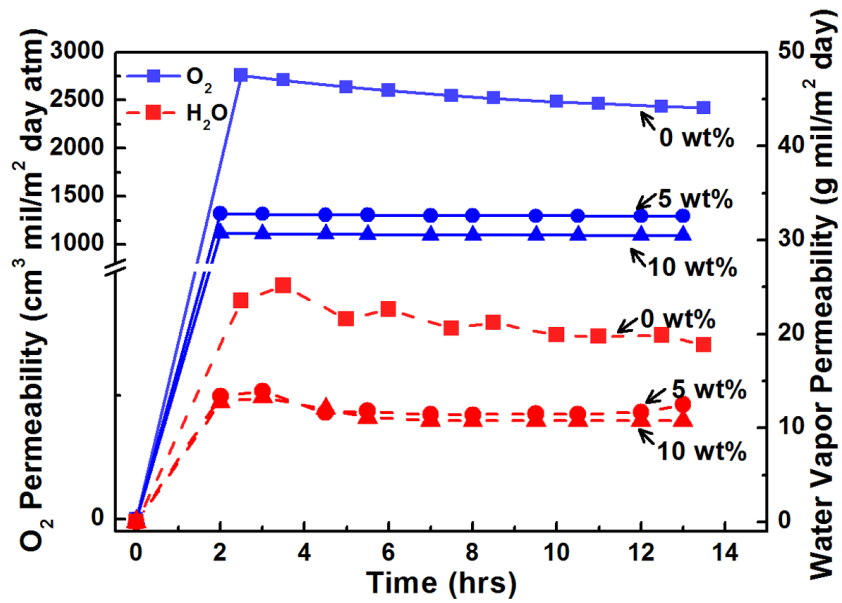


**Figure S13.** Experimental data showing the permeability of the nanocomposite films.

### Calculation of relative permeability by modified-Nielsen model

The addition of *f*-BNNPs to a pristine polymer would reduce gas solubility, due to the insolubility of gas in the sheets, and diffusivity, as the gas molecules must maneuver around the newly introduced impermeable two-dimensional nanofiller to diffuse through the polymer.<sup>1</sup> While a change in gas solubility as the addition of nanofillers is normally considered to be only dependent upon the volume fraction of the nanofiller ( $\phi_c$ ), diffusivity is also affected by the aspect ratio ( $\alpha$ ) of the two-dimensional barriers. Both parameters can be incorporated into a modified Nielsen model.<sup>2</sup> For non-uniform orientation of the platelets an order parameter,  $S'$ , is introduced to quantify the degree of their orientation around the diffusion direction.<sup>3</sup>

$$S' = \frac{1}{2} \langle 3 \cos^2 \theta - 1 \rangle \quad (1)$$

where  $\theta$  is the angle between the diffusion direction and the unit vector normal to the surface of a platelet, and the average is taken over all platelets with all possible orientations. When all platelets are random orientation, then the order parameter is  $S' = 0$ . For non-uniform orientation modified Nielsen's equation takes the following form:<sup>3</sup>

$$\frac{P_{composite}}{P_{matrix}} = \frac{1 - \phi_c}{1 + \frac{\alpha}{2} \frac{2}{3} \left( S' + \frac{1}{2} \right) \phi_c} \quad (2)$$

The theoretical permeability of the composites can be calculated from the modified Neilson equation (Equation 2). To convert weight fraction to volume fraction, the density of *f*-BNNPs was estimated based on the known density of bulk h-BN (2.1 g/cm<sup>3</sup>) and the density of the polyethylene matrix was determined to be 0.918 g/cm<sup>3</sup>.

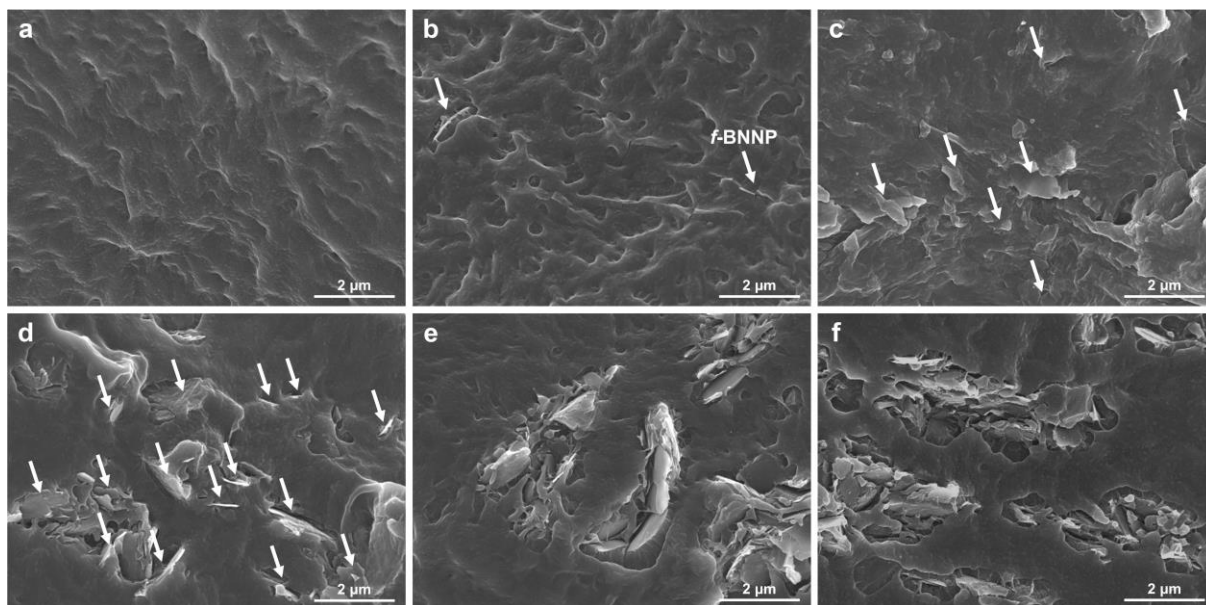


**Figure S14.** SEM images of the liquid-nitrogen-cooled fracture surfaces of the nanocomposites. a) pure polyethylene, b) 1 wt% *f*-BNNPs, c) 3 wt% *f*-BNNPs, d) 5 wt% *f*-BNNPs, e) 7 wt% *f*-BNNPs, and f) 10 wt% *f*-BNNPs.

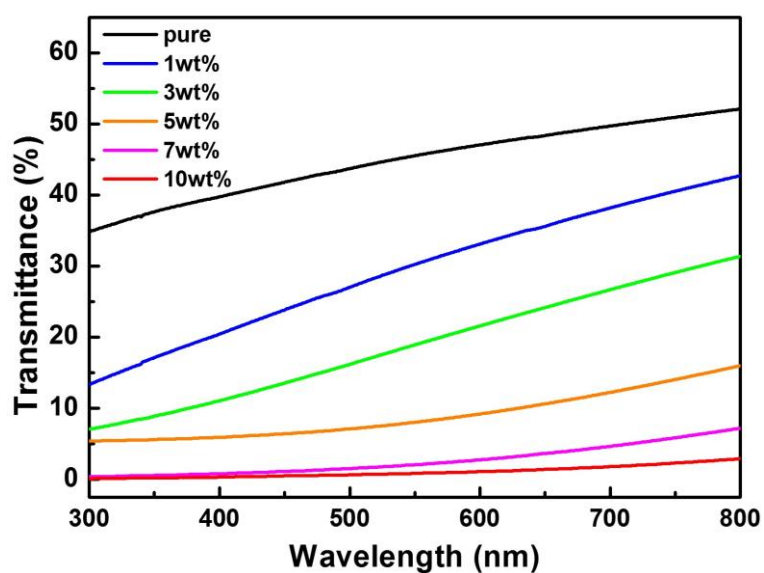


**Figure S15.** Optical transmittance of the nanocomposites.

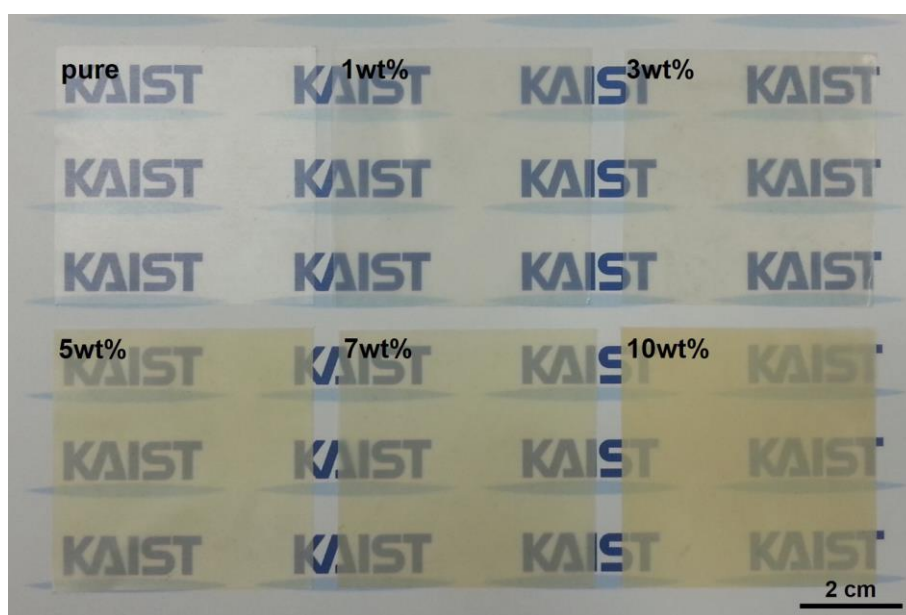


**Figure S16.** Photographs of the *f*-BNNPs/polyethylene nanocomposites for high-performance barrier films. The characters beneath the nanocomposites are legible through the specimens.

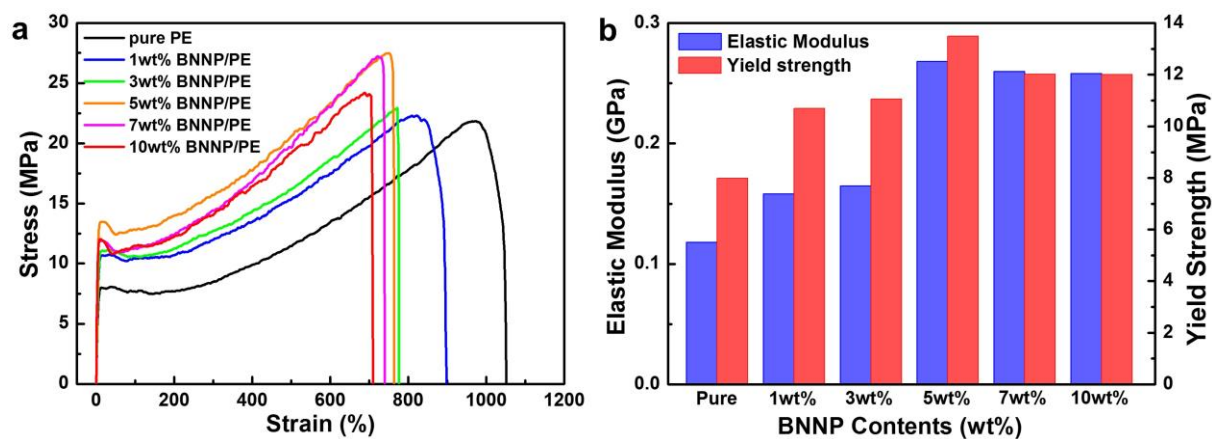


**Figure S17.** a) Stress–strain curves for the polyethylene nanocomposites. b) The elastic modulus and yield strength of the nanocomposites.

## REFERENCES

1. Compton, O. C.; Kim, S.; Pierre, C.; Torkelson, J. M.; Nguyen, S. T. *Adv. Mater.* **2010**, *22*, 4759–4763.
2. Choudalakis, G.; Gotsis, A. D. *Eur. Polym. J.* **2009**, *45*, 967–984.
3. Bharadwaj, R. K. *Macromolecules* **2001**, *34*, 9189–9192.